Earth and Planetary Science Letters 579 (2022) 117335

Contents lists available at ScienceDirect

Earth and Planetary Science Letters

www.elsevier.com/locate/epsl

Tidal modulation of seismicity at the Coso geothermal field

Wei Wang [a,b,*], Peter M. Shearer [a], John E. Vidale [b], Xiaohua Xu [c], Daniel T. Trugman [d], Yuri Fialko [a]

[a] Scripps Institution of Oceanography, University of California, San Diego, La Jolla, CA, USA
[b] Department of Earth Sciences, University of Southern California, Los Angeles, CA, USA
[c] Institute for Geophysics, University of Texas at Austin, Austin, TX, USA
[d] Jackson School of Geosciences, The University of Texas at Austin, Austin, TX, USA

ARTICLE INFO

Article history:
Received 12 June 2021
Received in revised form 30 November 2021
Accepted 5 December 2021
Available online 3 January 2022
Editor: H. Thybo

Dataset link: https://scedc.caltech.edu/eq-catalogs/index.html

Dataset link: https://igppweb.ucsd.edu/~agnew/Spotl/spotlmain.html

Keywords:
tidal triggering of earthquakes
tensile tidal stress
Coso geothermal field
remote triggering of earthquakes

ABSTRACT

Studying the seismicity triggering response of fault systems to periodic stress fluctuations can improve our understanding of earthquake nucleation, rupture failure processes, and local stress states. Geothermal fields are well known to be susceptible to triggering, as the injection and extraction activities change the local stress and fluid flow conditions. Here, we examine the modulation of earthquakes by Earth tides within California's Coso geothermal field (CGF) and its vicinity. To maximize our resolution to detect modulation of small earthquakes, we take advantage of the new Quake Template Matching catalog in southern California, which has nearly twice as many events in the Coso region as the standard catalog and is complete down to about magnitude 0.3. We observe strong tidal triggering of earthquakes within the CGF, even though the fluctuations of tidal stresses are small (~2 kPa). The tidally-triggered earthquakes tend to occur near the time of maximum tensile tidal stress. The signal is strongest near the edges of the zone of new production wells, suggesting fluid pressure gradients encourages triggering at tidal periods.

1. Introduction

A key and long-standing question in seismology is how earthquakes are triggered by stress changes, and in detail, how sensitive the triggering is to the amplitude and time scale of the stress variations (i.e., the period in the case of cyclical loading), and what this reveals about earthquake nucleation mechanisms. The continental crust is thought to be pervasively on the verge of failure (Zoback and Zoback, 2002) and temporal stress fluctuations may initiate earthquake nucleation either directly or by modulating the effective normal stress via fluid transport and pore-pressure changes (Gomberg et al., 1997; Hill and Prejean, 2007; Delorey et al., 2017; Thomas et al., 2009). If so, earthquake modulation should result from sufficiently large stress perturbations.

Two of the most widely studied examples of earthquake triggering due to periodic or quasi-periodic stress fluctuations involve triggering by earthquake shaking and Earth tides. Dynamic triggering from the seismic waves of distant earthquakes occurs at scales of tenths of a second to tens of seconds (frequencies of ~0.1-10 Hz), whereas triggering caused by Earth tides occurs over hours to days (~10^{-4}-10^{-6} Hz). Remote triggering from seismic shaking has been observed worldwide for over two decades, appearing most commonly in geothermal and volcanic areas (Hill et al., 1993; Gomberg and Davis, 1996; Prejean et al., 2004; Brodsky and Prejean, 2005; Peng et al., 2010; Aiken and Peng, 2014; Fan et al., 2021; Miyazawa et al., 2021). In contrast, studies of earthquake triggering by tides have a much longer history, but the results are mixed (e.g., Schuster, 1897; Vidale et al., 1998; Beeler and Lockner, 2003; Ader and Avouac, 2013; Wang and Shearer, 2015; Xue et al., 2018). Most of the well-documented examples of tidal triggering of earthquakes and tremors are observed near-shore or offshore, where the ocean loading term is up to ten times larger than the solid Earth tide (Cochran et al., 2004; Tanaka et al., 2002; Rubinstein et al., 2009; Métivier et al., 2009; Wilcock, 2009; Ide et al., 2016; Hao et al., 2019; Scholz et al., 2019), or in tremor-hosting fault zones where conditions of near-lithostatic fluid pressure may cause tidal modulation of tremor, low-frequency earthquakes, and slow earthquakes (Thomas et al., 2009, 2012; Houston, 2015). Measurement of robust statistical correlations between solid Earth tides and earthquake occurrence far from the oceans benefits from

* Corresponding author at: Department of Earth Sciences, University of Southern California, Los Angeles, CA, USA.
E-mail address: weiwang053@gmail.com (W. Wang).

https://doi.org/10.1016/j.epsl.2021.117335
0012-821X/

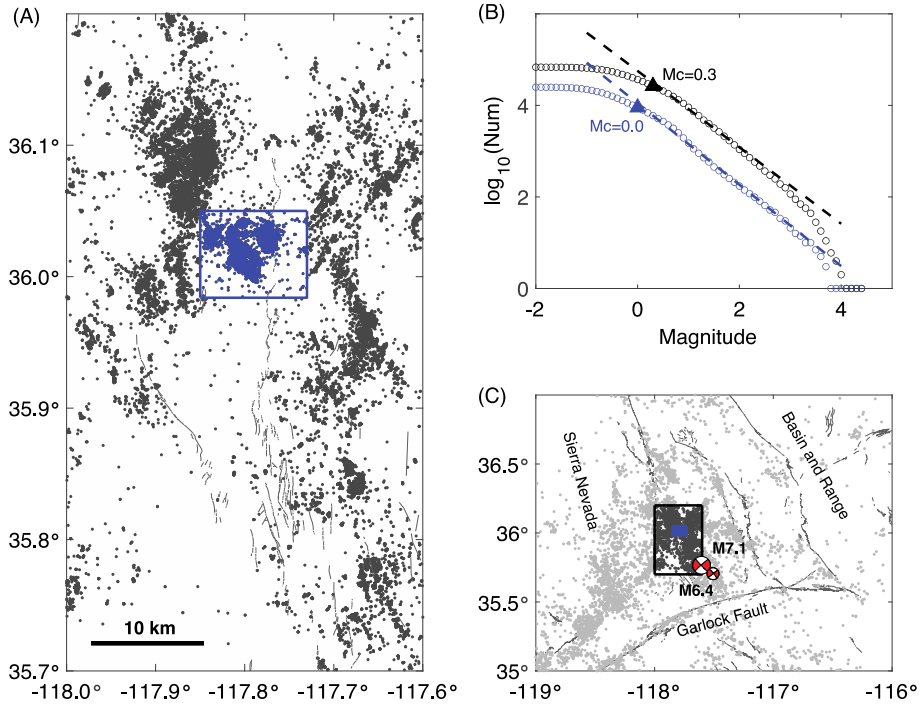

Fig. 1. Seismicity in the Coso geothermal field from 2008 to 2017. (A) shows seismicity in the CGF (blue) and its surrounding area (black, area in Fig. 1A). (B) illustrates the Gutenberg-Richter law in the CGF (blue) and its vicinity (black) for the QTM catalog, with triangles indicating the approximate completeness magnitudes. (C) shows the seismicity in eastern California, including the M6.4 and M7.1 Ridgecrest earthquakes. The black box indicates the same region in (A). (For interpretation of the colors in the figure(s), the reader is referred to the web version of this article.)

substantial improvements that augment earthquake catalogs (Métivier et al., 2009; Scholz et al., 2019).

Geothermal fields and volcanic areas are thought to be more susceptible to triggering phenomena because of their active tectonics, elevated temperature, and the presence of significant amounts of pore fluids at depth. In areas of geothermal energy production, continuous injection and extraction of fluids alters the stress state and fluid-flow conditions within the porous, complex fracture systems (e.g., Martínez-Garzón et al., 2013). In this study we focus on the Coso region in eastern California, which hosts one of the largest geothermal plants in the United States. The Coso geothermal field (CGF) is located between the Sierra Nevada and Argus Ranges, in the transtensional part of the Eastern California Shear Zone, which is subject to strike-slip as well as normal faulting (Walter and Weaver, 1980; Fialko, 2021; Fialko and Jin, 2021). The geothermal plant has been in operation since 1987 with a rated capacity of 270 MW (Monastero, 2002). The start of geothermal production at Coso triggered a notable increase in microseismicity within the production area (Fialko and Simons, 2000; Trugman et al., 2016).

2. Methodology and results

Tidal modulation studies require large numbers of events to ensure their statistical confidence (Harrington and Brodsky, 2006; Métivier et al., 2009; Scholz et al., 2019). The recently developed Quake Template Matching (QTM) catalog for southern California from 2008 to 2017 includes 1.8 million earthquakes (Ross et al., 2019), about a 10-fold increase from the Southern California Seismic Network (SCSN) catalog (Hutton et al., 2010). This enlarged catalog, with many more small events, improves our ability to detect statistically significant earthquake triggering over previous work (Vidale et al., 1998; Harrington and Brodsky, 2006). The completeness magnitudes in the CGF and its surroundings are approximately 0.0 and 0.3, respectively, compared to 0.5 for the SCSN catalog (see Figs. 1 & S1).

To examine the correlation between Earth tides and earthquake occurrence, we apply Schuster's test separately to different event sequences (Schuster, 1897). For a random sequence, the Schuster's p-value is defined as

$$p = \exp\left(-\left(\left(\sum_{i=1}^{N}\sin\theta_i\right)^2 + \left(\sum_{i=1}^{N}\cos\theta_i\right)^2\right)/N\right), \quad (1)$$

where θ_i is the tidal phase for the i-th event and N is the total number of events. We define the neighboring maximum values of the tidal stress signal as each occurring at 0° phase, as shown in Figure S2a, to estimate the tidal phase at the time of the earthquake. The p-value provides a measure of the probability that the observed correlation with tidal phase could happen by chance if earthquake occurrence was random. A p-value less than 5%, i.e., 0.05, is often taken to indicate a significant correlation between Earth tide amplitude and earthquake occurrence.

Schuster's test assumes each event is statistically independent of the other events. Thus temporal clustering in the seismicity, i.e., aftershock sequences and earthquake swarms, on the time scale of stressing period degrades the resolution to be worse than suggested by the p-value (e.g., Wang and Shearer, 2015). Consequently, we first use the Reasenberg declustering method (RDM) (Reasenberg, 1985), which identifies aftershocks by checking whether these events are located within the spatial and temporal interaction zone of a prior earthquake. The size and duration of the interaction zone increases with earthquake magnitude. Since there are some swarms without mainshocks in the Coso region (Zhang et al., 2017), and RDM may fail to identify and decluster swarms, we further apply the phase-bin declustering method (PBDM) (Wang and Shearer, 2015) to the RDM-declustered catalog. The PBDM declusters the catalog based on the tidal cycles, so it is only appropriate for tidal modulation studies. Each tidal cycle is divided into several equal-size bins, and only a single event in each bin is kept. This processing, for example, will not signal tidal correlation in any cycles with all bins fully occupied by at least an event.

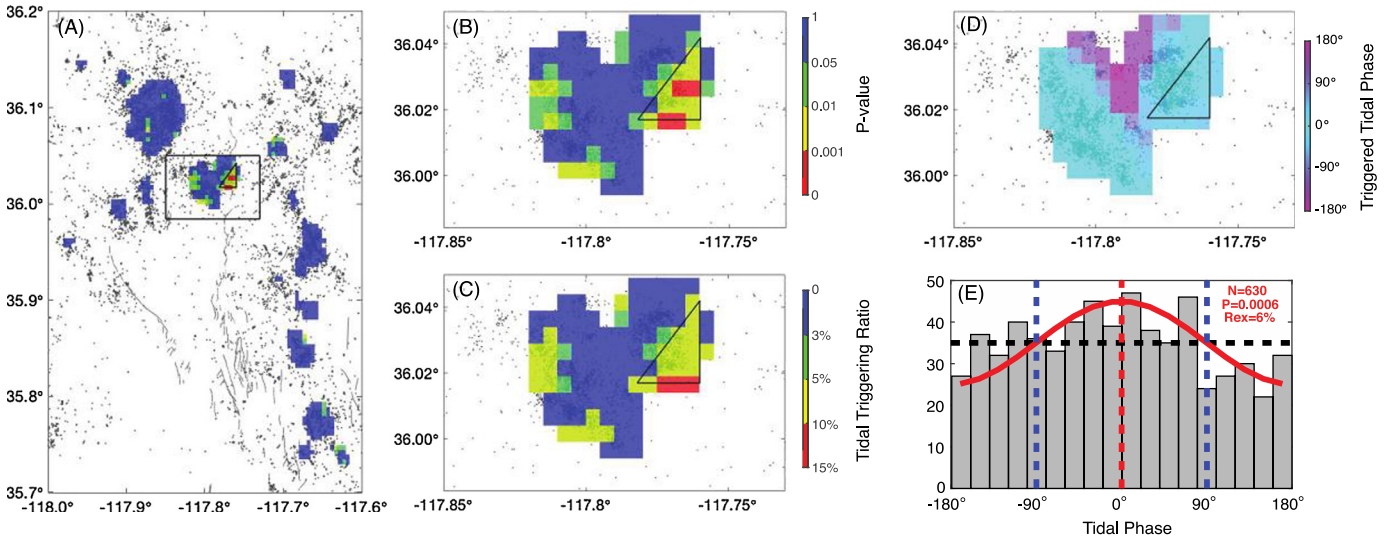

Fig. 2. Spatial variations in tidal triggering. (A) plots the p-value distribution for tidal triggering based on a 0.02° by 0.02° grid with shifts of 0.005°. (B) close-up view of the p-value distribution for tidal triggering within the black box in (A). (C) plots the tidal triggering ratios within the black box. (D) plots the triggered tidal phases within the black box. (E) a histogram illustrates the distribution of the tidal phases in the triangle region in (A)-(D), which shows a strong tidal modulation. The red solid line represents the best fitting cosine function, and the black dashed line shows the mean value.

The Earth tides are computed for the 2004 version of the Goddard Ocean Tide Model (GOT4.7) plus a local model for the west coast of the United States and British Columbia of Canada, using the program SPOTL (Agnew, 2012). In this study, PBDM is applied to the synthetic tidal signals from SPOTL, i.e., tensile tidal stress and tidal height in this study, which are dominated by the semi-diurnal periodicity. Hereafter, we use the term "tensile stress" to denote stress perturbations that result in a reduction in compressive stresses acting at depth (rather than the absolute extension).

Ideally, the geometry of the fault planes or the focal mechanisms of the triggered events would be used to relate tidal stress fluctuations to the shear and normal stress changes on the faults (Tanaka et al., 2002; Cochran et al., 2004; Johnson et al., 2017). However, both the local subsurface velocity and faulting processes are complex in our study region, which makes obtaining reliable focal mechanisms for the small events that make up the bulk of our catalog problematic (Martínez-Garzón et al., 2013). Therefore, we divide the study region into small geographic cells ($0.02° \times 0.02°$) (see Figs. 2 & 3), in which it is likely that the earthquakes will have similar focal mechanisms due to a near-uniform background tectonic stress state (Hardebeck, 2006; Wang and Shearer, 2015). These nearby events will be similarly affected by the common tidal phase.

Overall, we test the 595 cells that have at least 100 events in the greater CGF region (Fig. 2B). By random chance, we would expect 30 cells (5%) to have p-values below 0.05. In the observation, we find 54 cells with p-values below 0.05. 34 of 119 cells within CGF have p-values below 0.05, which is statistically significant, while only 4.2% of cells (20 out of 476) outside CGF have p-values smaller than 0.05. To be conservative in minimizing biases possible in iterated hypothesis testing, and since Schuster's test may overestimate significance (Cochran et al., 2004), we require a much lower p-value of 0.001 as a threshold to detect tidal modulation in our study region, which reduces the expected number of "random chance" cells to less than one out of 595. In contrast, we observe that 4 of all the cells have p-values less than 0.001 (values of 0.0001, 0.0001, 0.0003, and 0.0003) and that these cells are spatially proximate, with all of them located within the CGF. Similar to Cochran et al. (2004), we define the number of excess events ($N_{ex}=N_{obs}-N/2$, where N_{obs} is the observed number of events with $-90° < \theta < 90°$ and N is the total number of events) as the number beyond those expected due to random occurrences (see Figure S2b). The tidal triggering ratio is defined as $R_{ex}=N_{ex}/N$. In Fig. 2, R_{ex} for the subarea A is about 6%, while the tidal triggering is visibly apparent with a p-value equal to 0.0006, slightly smaller than 0.001.

We examine tidal modulation based on two different tidal components, tidal tensile stress (Fig. 2 & 3A-C), and tidal height (Fig. 3D). Both results indicate there is strong tidal triggering, i.e., $p < 0.001$, in the part of the CGF where there is observed long-term surface subsidence and highly active seismicity (Fialko and Simons, 2000; Tymofyeyeva and Fialko, 2015) (see Fig. 2 & 4). This anomaly is distinct from its surroundings, as the only extremely low p-value region is located in the CGF. Triggering appears to occur in phase with tensile stress, with the strongest triggering response concurrent with the greatest tensile stress (Fig. 2 & 4), which corresponds to the greatest extension. In the CGF, about 95% of earthquakes are shallow (<3 km) and proximate to geothermal operations (Fialko and Simons, 2000; Zhang et al., 2017). The tidal triggering of earthquakes for only these shallow events, shown in Fig. 3C, is very similar to the events across the entire depth range (see Fig. 3B).

For comparison, we repeated our analyses using only the SCSN catalog within the CGF. We found that the probability of tidal triggering and the tidal triggering ratio were lower than the QTM catalog results (see Fig. 3F). The detection of statistically significant tidal triggering at the CGF requires the large number of low magnitude ($M < 0.5$) earthquakes in the QTM catalog, as the SCSN catalog cannot confirm a significant tidal signal using only magnitude 0.5 or larger events.

3. Discussion

3.1. Statistical tests

As in previous studies (Schuster, 1897; Tanaka et al., 2002; Cochran et al., 2004; Wang and Shearer, 2015), we use the p-value to resolve tidal modulation of earthquakes. However, because we are testing many different cells, we use a much smaller p-value (0.001 or 0.1%) as the threshold value instead of the classic one ($p < 0.05$) to avoid bias from "P-hacking" and assure the confidence of our results. As discussed above, we find four cells with these extremely low p-values, which are located within a somewhat larger

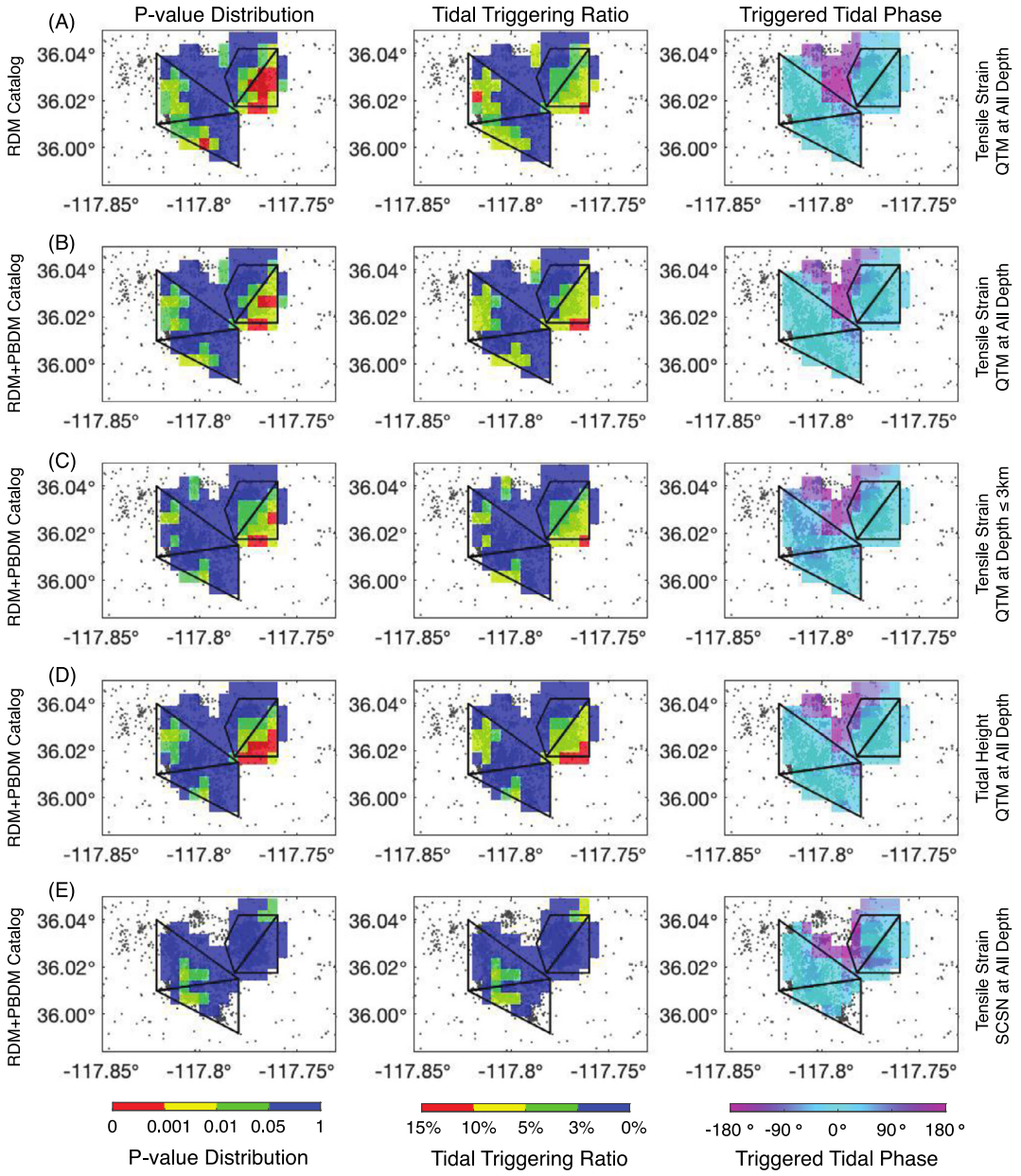

Fig. 3. Spatial variations in tidal triggering parameters including the p-value, tidal triggering ratio and triggered tidal phase. (A) shows the tidal triggering of tensile stress in the RDM declustered QTM catalog at all depths. (B) shows the tidal triggering of tensile stress in the RDM and PBDM declustered QTM catalog at all depths. (C) shows the tidal triggering of tensile stress in the RDM and PBDM declustered QTM catalog at depth $\leq$ 3 km. (D) shows the tidal triggering of tidal height in the RDM and PBDM declustered QTM catalog at all depths. (E) shows the tidal triggering of tensile stress in the RDM and PBDM declustered SCSN catalog at all depths.

region of 15 cells in the GCF containing p-values between 0.01 to 0.05, as indicated by the triangle in Fig. 2. Testing only the 630 earthquakes within this triangle for tidal triggering yields a p-value of 0.0006, confirming the anomalous nature of this region. All the cells with $p < 0.001$ in Fig. 3 have tidal triggering ratios (R_{ex}) larger than 5%.

To examine the spatial robustness of the low p-value regions, we randomly pick one event and find its closest neighboring 200 or 500 events, then we apply PBDM to this cluster and compute its p-value. We repeat this process 2000 times ($>1/0.001$ to check the location of the extremely low p-values). After repeating this process many times, the results indicate that the extremely low p-values are almost all located in the CGF (see Fig. 5A & B). In some cases, there may be extremely low p-values outside the CGF, however, the most robust spatial locations of the low p-values are within the CGF region. Second, we pick 5 random calendar years in the dataset and run the same process described above to check the location of the extreme low p-values. The results are similar to those of the whole dataset (see Fig. 5C & D). The spatial distribution of low p-values is more compact for the 500-event clusters than the 200-event clusters, suggesting the distribution in the 200-event clusters may be picking up random statistical fluctuations or more local or undersampled triggering regions.

3.2. Remote triggering

Remote triggering from the stress fluctuations in passing seismic waves is another tool for studying earthquake triggering (e.g., Gomberg et al., 1997; Hill and Prejean, 2007; Pollitz et al., 2012; Fan et al., 2021; Miyazawa et al., 2021) as well as aseismic slip events (e.g., Tymofyeyeva et al., 2019). Dynamic triggering from local and distant earthquakes typically occurs for seismic waves with

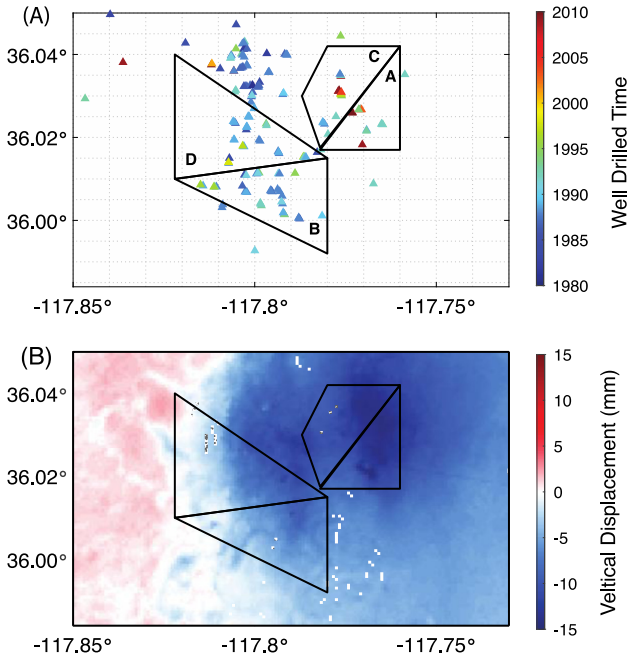

Fig. 4. (A) indicates geothermal well drilling date. (B) shows the surface displacement, as derived from InSAR data of Sentinel-1 between November 2014 and December 2017 in the black box in Fig. 2A. The subareas are the same as those in Fig. 3. The subarea A is the region with a strong tidal modulation, while C is the one with almost none tidal modulation. The subarea B and D are the regions with a medium tidal modulation.

periods of seconds to tens of seconds (frequencies of 0.1-10 Hz). Previous remote triggering studies in the CGF have obtained different results despite using similar methodology (Aiken and Peng, 2010; Zhang et al., 2016; Kaven, 2020; Alfaro-Diaz et al., 2020; Im et al., 2021).

Aiken and Peng (2014) and Alfaro-Diaz et al. (2020) examined the triggering of earthquakes by transient stresses caused by seismic waves from distant earthquakes at the stations located within and/or close to the CGF. Both studies confirm the triggering of earthquakes within the CGF. However, Aiken and Peng (2014) found only stress perturbations larger than 5 kPa can trigger the earthquakes within the CGF, while Alfaro-Diaz et al. (2020) suggested the remote triggering may depend on the orientation of the transient dynamic stress rather than simply the amplitude.

Zhang et al. (2017), applied the β-statistics method to the RDM SCSN catalog and found no evidence of remote triggering within the CGF but confirmed remote triggering nearby outside the field itself for the 1992 Landers earthquake. In contrast, Kaven (2020) detected remote triggering behavior following the 2019 Ridgecrest earthquake using the Navy Geothermal Program Office catalog, also using the same β-statistics method. In the supplement, we confirm remote triggering within CGF using the RDM QTM catalog, but find that the patterns of remote triggering are complicated and not as consistent as tidal triggering at CGF.

3.3. Possible mechanisms

We find that tidal modulation of earthquakes consistently occurs in the CGF but not its immediate surroundings, whereas dynamic triggering from distant earthquakes is only sometimes detected within the GCF (Aiken and Peng, 2010; Zhang et al., 2016; Kaven, 2020; Alfaro-Diaz et al., 2020; Im et al., 2021). What could account for this behavior?

The continuous extraction of hot water out of a geothermal reservoir and the injection of cold water into it causes deflation of the reservoir due to cooling and net extraction. We compare the injection, production, and net production data with the declustered seismicity within the CGF. The temporal correlations between the seismicity and these parameters are very weak (see Figure S3), as observed by Trugman et al. (2016). In addition, there is no significant difference in seismicity between local day and night times (see Figure S4). Consistent with the Coso geothermal plants operating nearly 24 hours a day, seven days a week, and the weak correlation between the seismicity and anthropogenic activities, no day and night difference is apparent in our triggering results.

Within the CGF, we observe that the earthquakes preferentially occur near times of maximum tensile tidal stress. This result is consistent with most events occurring on normal and strike-slip faults caused by deflation of the geothermal reservoir, events that would be triggered by horizontal tensile stress (Fialko and Simons, 2000; Yu et al., 2018). It should be noted that the tensile tidal stresses on continents are very small (~2 kPa, estimated from the peak tensile tidal strain assuming a Poisson solid with shear modulus 30 GPa).

Our observations of tidal modulation of earthquakes imply that any pore-pressure homogenization that occurs in the Coso production region, as proposed by Zhang et al. (2017) to inhibit dynamic triggering, and the thermal destressing proposed by Im et al. (2021) does not prevent triggering at tidal periods. One possibility is that the unclogging process described by Zhang et al. (2017) facilitates stress-driven fluid flow over longer distances than is typical for fracture systems outside the Coso field, making possible fluid flow over many hours that could alter the effective stress on faults enough to trigger earthquakes. In this respect, it is interesting that the strongest tidal triggering signal at Coso clearly occurs near the edge of the area of new active production (see Fig. 3 & 4), where one might expect pore pressure gradients as one moves away from the injection wells. Another possibility is that host rocks in the production area are on the verge of failure at all times so that triggering is modulated by small variations in the pore fluid pressure (e.g., due to sub-daily variations in the extraction and injection rates). In this case, the rate of remote triggering would be determined by the probability of favorable fluid pressure at the time of passage of seismic waves. The probability may be low for any given teleseismic or regional event. Stress changes caused by tides, on the other hand, occur over much longer intervals, and thus are nearly continually superposed on any local fluctuations in the fluid pressure. Testing of this hypothesis would benefit from data on sub-daily variations in the pore fluid pressure, which currently is unavailable to the general public.

CRediT authorship contribution statement

Conception and design of study: Wei Wang, Peter M. Shearer;
Analysis of data: Wei Wang, Xiaohua Xu, Daniel Trugman;
Drafting the manuscript: Wei Wang, Peter M. Shearer, John E. Vidale, Xiaohua Xu, Daniel T. Trugman, Yuri Fialko;
All persons who meet authorship criteria are listed as authors, and all authors certify that they have participated sufficiently in the work to take public responsibility for the content, including participation in the concept, design, analysis, writing, or revision of the manuscript. Furthermore, each author certifies that this material or similar material has not been and will not be submitted to or published in any other publication before its appearance in the Earth and Planetary Science Letter.

Declaration of competing interest

The authors declare that they have no known competing financial interests or personal relationships that could have appeared to influence the work reported in this paper.

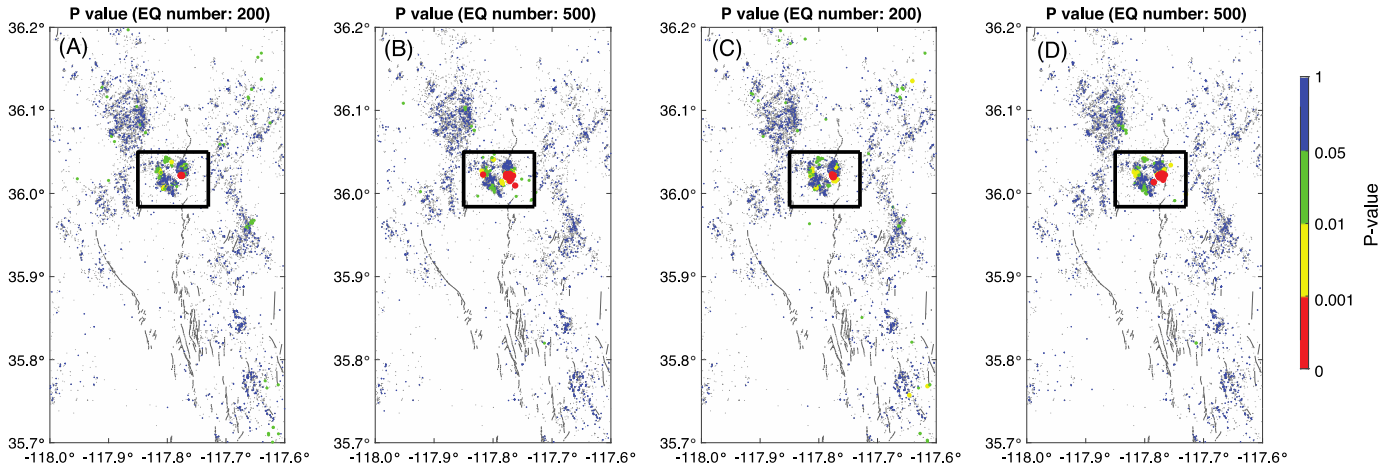

Fig. 5. Results of statistical tests, (A) and (B) show the p-value distributions of 2000 clusters from one randomly picked event from across the whole study area and its closest 200 and 500 events, respectively. (C) and (D) show the p-value distributions of 2000 clusters from one randomly picked event and its closest 200 and 500 events from a random 5 calendar years of data, respectively.

Data availability

The SCSN and QTM catalogs can be found at the website https://scedc.caltech.edu/eq-catalogs/index.html. The program to compute the tidal loading is downloaded from the website https://igppweb.ucsd.edu/~agnew/Spotl/spotlmain.html.

Acknowledgements

We thank the editor Hans Thybo, Roland Bürgmann and an anonymous reviewer for their fruitful and constructive comments, which greatly improved the manuscript. We thank Duncan Agnew for his discussion on the statistical tests and tidal triggering, Adrian Borsa and Sylvian Barbot for their helpful discussion. We also thank Zachary Ross and Egill Hauksson for discussion about the QTM catalog and for guidance in template matching techniques.

Funding: Funding for this research was provided by NEHRP/USGS grant G18AP00024.

Appendix A. Supplementary material

Supplementary material related to this article can be found online at https://doi.org/10.1016/j.epsl.2021.117335.

References

Ader, T.J., Avouac, J.P., 2013. Detecting periodicities and declustering in earthquake catalogs using the Schuster spectrum, application to Himalayan seismicity. Earth Planet. Sci. Lett. 377–378, 97–105.

Agnew, D.C., 2012. Scripps Institution of Oceanography Technical Report SPOTL: Some Programs for Ocean-Tide Loading.

Aiken, C., Peng, Z., 2014. Dynamic triggering of microearthquakes in three geothermal/volcanic regions of California. J. Geophys. Res., Solid Earth 119, 6992–7009.

Alfaro-Diaz, R., Velasco, A.A., Pankow, K.L., Kilb, D., 2020. Optimally oriented remote triggering in the Coso Geothermal region. J. Geophys. Res., Solid Earth 125 (8), 1–18.

Beeler, N.M., Lockner, D.A., 2003. Why earthquakes correlate weakly with the solid Earth tides: effects of periodic stress on the rate and probability of earthquake occurrence. J. Geophys. Res. 108 (B8).

Brodsky, E.E., Prejean, S.G., 2005. New constraints on mechanisms of remotely triggered seismicity at Long Valley Caldera. J. Geophys. Res., Solid Earth 110 (4), 1–14.

Cochran, E.S., Vidale, J.E., Tanaka, S., 2004. Earth tides can trigger shallow thrust fault earthquakes. Science 306 (5699), 1164–1166.

Delorey, A.A., van der Elst, N.J., Johnson, P.A., 2017. Tidal triggering of earthquakes suggests poroelastic behavior on the San Andreas Fault. Earth Planet. Sci. Lett. 460, 164–170.

Fan, W., Barbour, A.J., Cochran, E.S., Lin, G., 2021. Characteristics of frequent dynamic triggering of microearthquakes in Southern California. J. Geophys. Res., Solid Earth 126 (1), 1–28.

Fialko, Y., 2021. Estimation of absolute stress in the hypocentral region of the 2019 Ridgecrest, California, earthquakes. J. Geophys. Res., Solid Earth 126 (7), e2021JB022000.

Fialko, Y., Jin, Z., 2021. Simple shear origin of the cross-faults ruptured in the 2019 Ridgecrest earthquake sequence. Nat. Geosci. 14, 513–518.

Fialko, Y., Simons, M., 2000. Deformation and seismicity in the Coso geothermal area, Inyo County, California: observations and modeling using satellite radar interferometry. J. Geophys. Res., Solid Earth 105 (B9), 21781–21793.

Gomberg, J., Blanpied, M.L., Beeler, M., 1997. Transient triggering of near and distant earthquakes. Bull. Seismol. Soc. Am. 87 (2), 294–309.

Gomberg, J., Davis, S., 1996. Stress/strain changes and triggered seismicity at the geysers, California. J. Geophys. Res., Solid Earth 101 (1), 733–749.

Hardebeck, J.L., 2006. Homogeneity of small-scale earthquake faulting, stress, and fault strength. Bull. Seismol. Soc. Am. 96 (5), 1675–1688.

Hao, J., Zhang, J., Yao, Z., 2019. Evidence for diurnal periodicity of earthquakes from midnight to daybreak. Nat. Sci. Rev. 6 (5), 1016–1023.

Harrington, R.M., Brodsky, E.E., 2006. The absence of remotely triggered seismicity in Japan. Bull. Seismol. Soc. Am. 96 (3), 871–878.

Hill, D.P., Reasenberg, P.A., Michael, A., Arabaz, W.J., Beroza, G., Brumbaugh, D., et al., 1993. Seismicity remotely triggered by the magnitude 7.3 Landers, California, earthquake. Science 260 (5114), 1617–1623.

Hill, D.P., Prejean, S.G., 2007. Dynamic triggering. In: Treatise on Geophysics, Vol. 4, pp. 257–291.

Houston, H., 2015. Low friction and fault weakening revealed by rising sensitivity of tremor to tidal stress. Nat. Geosci. 8, 409–415.

Hutton, K., Woessner, J., Hauksson, E., 2010. Earthquake monitoring in southern California for seventy-seven years (1932-2008). Bull. Seismol. Soc. Am. 100 (2), 423–446.

Ide, S., Yabe, S., Tanaka, Y., 2016. Earthquake potential revealed by tidal influence on earthquake size-frequency statistics. Nat. Geosci. 9 (11), 834–837.

Im, K., Avouac, J.P., Heimisson, E.R., et al., 2021. Ridgecrest aftershocks at Coso suppressed by thermal destressing. Nature 595, 70–74.

Johnson, C.W., Fu, Y., Bürgmann, R., 2017. Stress models of the annual hydrospheric, atmospheric, thermal, and tidal loading cycles on California faults: perturbation of background stress and changes in seismicity. J. Geophys. Res., Solid Earth 122, 10,605–10,625.

Kaven, J.O., 2020. Seismicity rate change at the Coso Geothermal field following the July 2019 ridgecrest earthquakes. Bull. Seismol. Soc. Am. 110 (4), 1728–1735.

Martínez-Garzón, P., Bohnhoff, M., Kwiatek, G., Dresen, G., 2013. Stress tensor changes related to fluid injection at the geysers geothermal field, California. Geophys. Res. Lett. 40 (11), 2596–2601.

Métivier, L., de Viron, O., Conrad, C.P., Renault, S., Diament, M., Patau, G., 2009. Evidence of earthquake triggering by the solid Earth tides. Earth Planet. Sci. Lett. 278 (3–4), 370–375.

Miyazawa, M., Brodsky, E.E., Guo, H., 2021. Dynamic earthquake triggering in Southern California in high resolution: intensity, time decay, and regional variability. AGU Adv. 2 (2). e2020AV000309.

Monastero, F.C., 2002. An overview of industry military cooperation in the development of power operations at the Coso Geothermal Field in southern California. Geotherm. Resour. Counc. Bull. 31 (5), 188–195.

Peng, Z., Hill, D.P., Shelly, D.R., Aiken, C., 2010. Remotely triggered microearthquakes and tremor in central California following the 2010 Mw8.8 Chile earthquake. Geophys. Res. Lett. 37 (24), 2–7.
Pollitz, F., Stein, R., Sevilgen, V., Bürgmann, R., 2012. The 11 April 2012 East Indian Ocean earthquake triggered large aftershocks worldwide. Nature 490, 250–253.
Prejean, S.G., Hill, D.P., Brodsky, E.E., Hough, S.E., Johnston, M.J.S., Malone, S.D., Oppenheimer, D.H., Pitt, A.M., Richards-Dinger, K.B., 2004. Remotely triggered seismicity on the United States west coast following the Mw 7.9 Denali fault earthquake. Bull. Seismol. Soc. Am. 94 (6 Suppl. B), 348–359.
Reasenberg, P., 1985. Second-order moment of central California seismicity, 1969-1982. J. Geophys. Res. 90, 5479–5495.
Ross, Z.E., Trugman, D.T., Hauksson, E., Shearer, P.M., 2019. Searching for hidden earthquakes in Southern California. Science 6 (1), 1–46.
Scholz, C.H., Tan, Y.J., Albino, F., 2019. The mechanism of tidal triggering of earthquakes at mid-ocean ridges. Nat. Commun. 10 (1), 1–7.
Schuster, A., 1897. On lunar and solar periodicities of earthquakes. Proc. R. Soc. 61 (369–377), 455–465.
Tanaka, S., Ohtake, M., Sato, H., 2002. Evidence for tidal triggering of earthquakes as revealed from statistical analysis of global data. J. Geophys. Res., Solid Earth 107 (B10), 1–1-ESE 1-11.
Thomas, A., Nadeau, R., Bürgmann, R., 2009. Tremor-tide correlations and near-lithostatic pore pressure on the deep San Andreas fault. Nature 462, 1048–1051.
Thomas, A.M., Bürgmann, R., Shelly, D.R., Beeler, N.M., Rudolph, M.L., 2012. Tidal triggering of low frequency earthquakes near Parkfield, California: implications for fault mechanics within the brittle-ductile transition. J. Geophys. Res. 117, B05301.
Trugman, D.T., Shearer, P.M., Borsa, A.A., Fialko, Y., 2016. A comparison of long-term changes in seismicity at the Geysers, Salton Sea, and Coso geothermal fields. J. Geophys. Res., Solid Earth 121 (1), 225–247.
Tymofyeyeva, E., Fialko, Y., 2015. Mitigation of atmospheric phase delays in InSAR data, with application to the eastern California shear zone. J. Geophys. Res., Solid Earth 120 (8), 5952–5963.
Tymofyeyeva, E., Fialko, Y., Jiang, J., Xu, X., Sandwell, D., Bilham, R., et al., 2019. Slow slip event on the Southern San Andreas fault triggered by the 2017 Mw 8.2 Chiapas (Mexico) earthquake. J. Geophys. Res., Solid Earth 124, 9956–9975.
Vidale, J.E., Agnew, D.C., Johnston, M.J.S., Oppenheimer, D.H., 1998. Absence of earthquake correlation with Earth tides: an indication of high preseismic fault stress rate. J. Geophys. Res., Solid Earth 103 (B10), 24567–24572.
Walter, A.W., Weaver, C.S., 1980. Seismicity of the Coso Range, California. J. Geophys. Res. 85 (B5), 2441–2458.
Wang, W., Shearer, P.M., 2015. No clear evidence for localized tidal periodicities in earthquakes in the central Japan region. J. Geophys. Res., Solid Earth 120 (9), 6317–6328.
Wilcock, W.S.D., 2009. Tidal triggering of earthquakes in the Northeast Pacific Ocean. Geophys. J. Int. 179 (2), 1055–1070.
Xue, L., Bürgmann, R., Shelly, D.R., Johnson, C.W., Taira, T., 2018. Kinematics of the 2015 San Ramon, California earthquake swarm: implications for fault zone structure and driving mechanisms. Earth Planet. Sci. Lett. 489, 135–144.
Yu, C., Vavryčuk, V., Adamová, P., Bohnhoff, M., 2018. Moment tensors of induced microearthquakes in the Geysers geothermal reservoir from broadband seismic recordings: implications for faulting regime, stress tensor, and fluid pressure. J. Geophys. Res., Solid Earth 123 (10), 8748–8766.
Zhang, Q., Lin, G., Zhan, Z., Chen, X., Qin, Y., Wdowinski, S., 2017. Absence of remote earthquake triggering within the Coso and Salton Sea geothermal production fields. Geophys. Res. Lett. 44 (2), 726–733.
Zoback, M.D., Zoback, M.L., 2002. Stress in the Earth's Lithosphere. Encyclopedia of Physical Science and Technology, vol. 16, pp. 143–154.

Supplementary material for "Tidal modulation of seismicity at the Coso geothermal field"

Wei Wang[1,2*], Peter M. Shearer[1], John E. Vidale[2], Xiaohua Xu[1], Daniel T. Trugman[3], Yuri Fialko[1]

[1]Scripps Institution of Oceanography, University of California, San Diego, La Jolla, California, USA.

[2]Department of Earth Sciences, University of Southern California, USA

[3]Jackson School of Geosciences, The University of Texas at Austin

*Correspondence to: weiwang053@gmail.com

This is the supplementary material for "Tidal modulation of seismicity at the Coso geothermal field" for the main text. Here we present the parameter selection for the declustering analysis. Second, we show the remote triggering in the Coso geothermal field (CGF) for the comparison of the tidal modulation within CGF. Furthermore, there are several plots to present the Gutenberg-Richter Law, the determination of tidal phase and preferred tidal phase, the comparison between the declustered seismicity and injection, production, the seismicity at day and night time, and results for remote triggering.

Parameters for declustering analysis

We used *Matthews and Reasenberg* (1985) to decluster the catalogs. The most critical parameter is the number of crack radii surrounding each earthquake within which to consider linking an event into the cluster, so for this we use 10, similar to *Kaven* (2020). We used -1 for the cut-off magnitude during clusters. In this declustering approach, we do not consider location error.

Remote Triggering

Here, we examine remote triggering by applying the β-statistics method [*Reasenberg and Simpson*, 1992] to the RDM QTM catalog from 2008 to 2017. The β-value is defined by the difference between the observed number of earthquakes in the study time window and the expected number based on the reference background seismicity, normalized by the standard deviation of the expected seismicity. The β-value is defined as, $\beta = [n_a - E(n_a; n_b)]/var(n_a; n_b)^{1/2}$, where $E(n_a; n_b) = n_b(t_a/t_b)$ is the expected number during window t_a based on the background seismicity within t_b and $var(n_a; n_b) = n_b(t_a/t_b)$ is the variance for a Poisson process. In this study, we use 200 days before the target earthquake to compute the background seismicity and the 10 days after it for the expected seismicity. A β-value larger than 2 or smaller than -2 indicates the presence or absence of remote triggering [*Reasenberg and Simpson*, 1992].

We search for distant earthquakes during the same period with Ms >= 6 in the Global Centroid Moment Tensor (GCMT) catalog from 2008 to 2017, the same interval as the QTM catalog. We examine all the distant earthquakes that can generate peak-ground velocity (PGV) over 0.1 mm/s within the CGF, similar to *Alfano-Diaz et al.* [2020]. The PGV can be estimated

using the equation, $\mathrm{PGV} = 2\pi/\mathrm{T} \times 10^{\mathrm{Ms}-1.66\mathrm{A}-2}$, in which Ms is the surface wave magnitude, A is the distance to the event (km), and T is surface-wave period (s) [*Lay and Wallace*, 1995]. The peak dynamic stress can be estimated using the equation $\sigma = \mu * PGV/c$, where c is the phase velocity (assumed to be 3 km/s), and μ is the shear modulus (assumed to be 30 GPa). In this case, the critical dynamic stress fluctuation we use to search is 1 kPa, equivalent to PGV 0.1 mm/s.

We examine the same spatial cell gridding as in the tidal triggering analysis described in Figure 2A. We look for statistically significant increases in seismicity rate using the β-statistics method for five distant earthquakes producing stress fluctuations larger than 5 kPa, i.e., PGV larger than 0.5 mm/s. Note that the 2010 El Mayor-Cucapah earthquake (EMC) (Ms=7.3) was by far the strongest, with estimated PGV over 4 cm/s. We find many examples of remote triggering and the results show that remote triggering is less likely to be observed within the CGF than its surroundings, i.e., the fraction of cells with a significant increase in seismicity rate within the CGF is significantly smaller than that in its surrounding region for all five events (see Figure S5A and S6). However, note that the cells with rate increases show little agreement among the different distant earthquakes. Given the number of cells we examine, it is possible that some apparently statistically significant increases in rate could occur from purely random variations in earthquake occurrence times. We examine this issue using a Monte Carlo test. For each cell, we apply the observed seismicity rate prior to each target event to generate a random earthquake sequence following the event, assuming earthquake occurrence times obey a Poisson distribution. Then, we compute the β-values for all the cells and find that none of the cells have a significant increase in seismicity rate (β-value>2), even if the entire procedure is repeated 100 times. This confirms the statistical significance of our dynamic triggering observations.

Overall, 15 out of 37 studied global earthquakes showed some evidence for remote triggering in the CGF. It should be noted that the number of events is limited and there is no conclusive relation between triggering and the azimuths of the events (Figure S7). Furthermore, there is no spatial consistency of the remote triggering within the CGF, unlike the tidal triggering (see Figure S5). However, notably the region with the strongest tidal triggering does not show much evidence for remote triggering. These observations suggest more complex and variable mechanisms for remote triggering at the CGF and its surroundings compared to the more consistent tidal triggering observed in the GCF.

Figure S1-S7

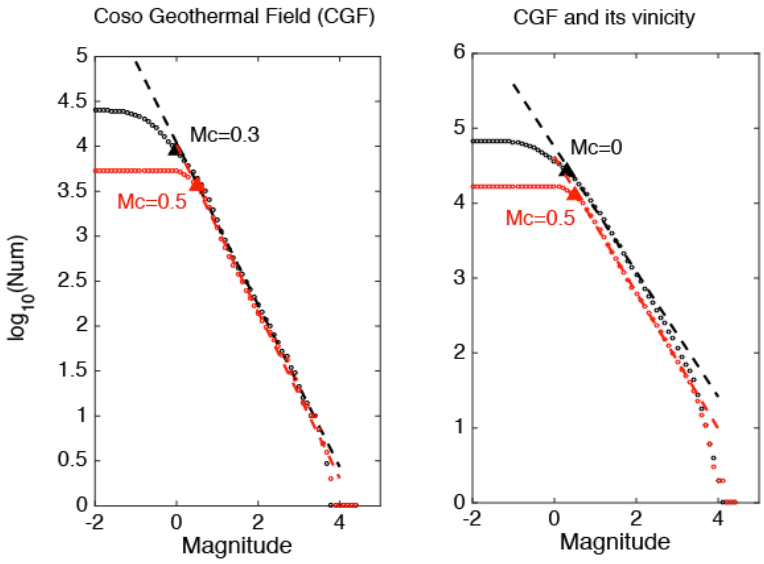

Figure S1. Comparison of the completeness magnitude of the Coso geothermal field (red) and its surroundings (black, area in Figure 1A) for SCSN catalog (red).

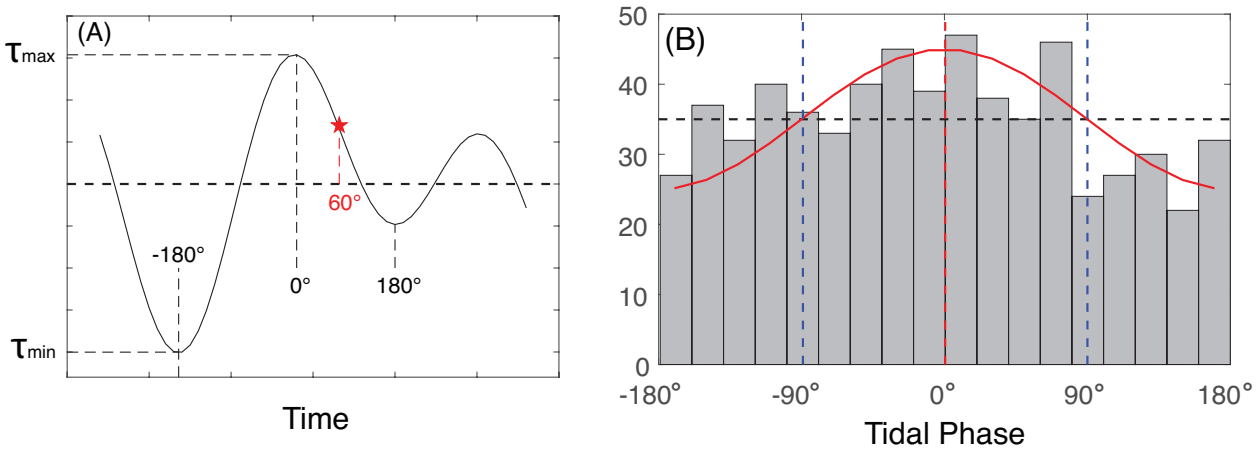

Figure S2. (A) A diagram of the tidal stress time series for an earthquake with tidal phase 60°. (B) The histogram of tidal phases for events in subarea A in Fig. 3. The red line is the best-fitting cosine function of the tidal phase distribution. The red dashed line marks the preferential tidal phase bin, and the two blue dashed lines mark the half cycle centered at the preferential tidal triggering phase.

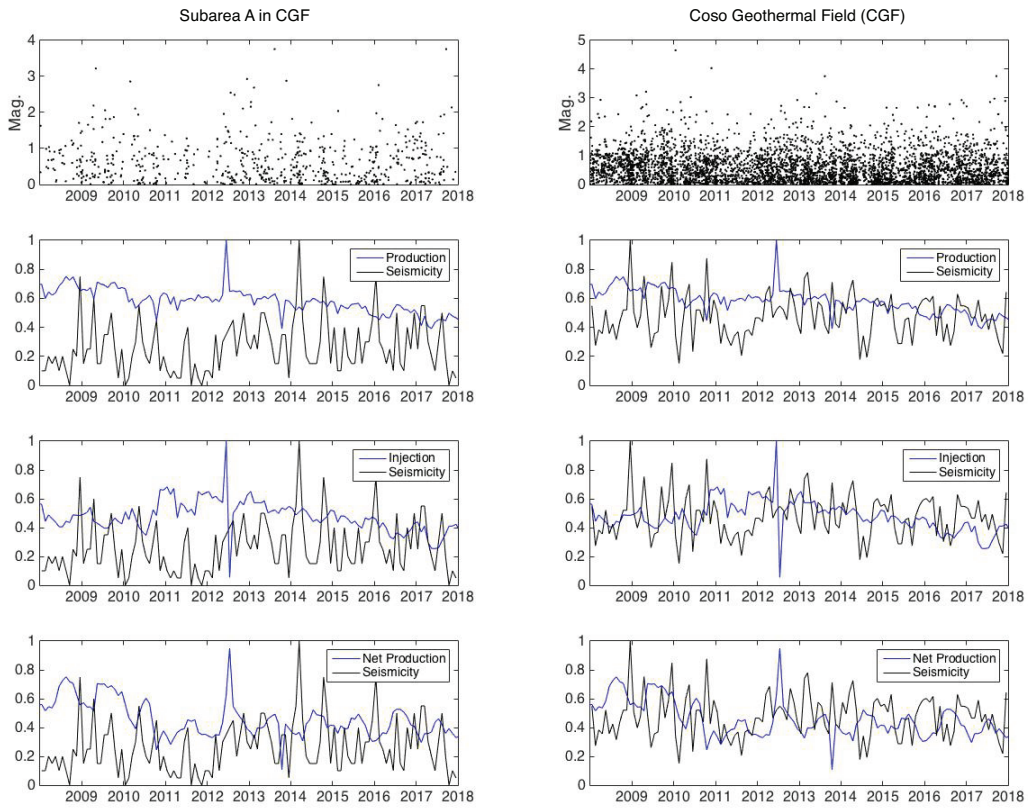

Figure S3. Comparison of declustered seismicity rate in the QTM catalog and production, injection and net production rate for the subarea A within the CGF and the whole CGF (see Figure 2). The seismicity, production, injection, and net production are normalized by their maximum values.

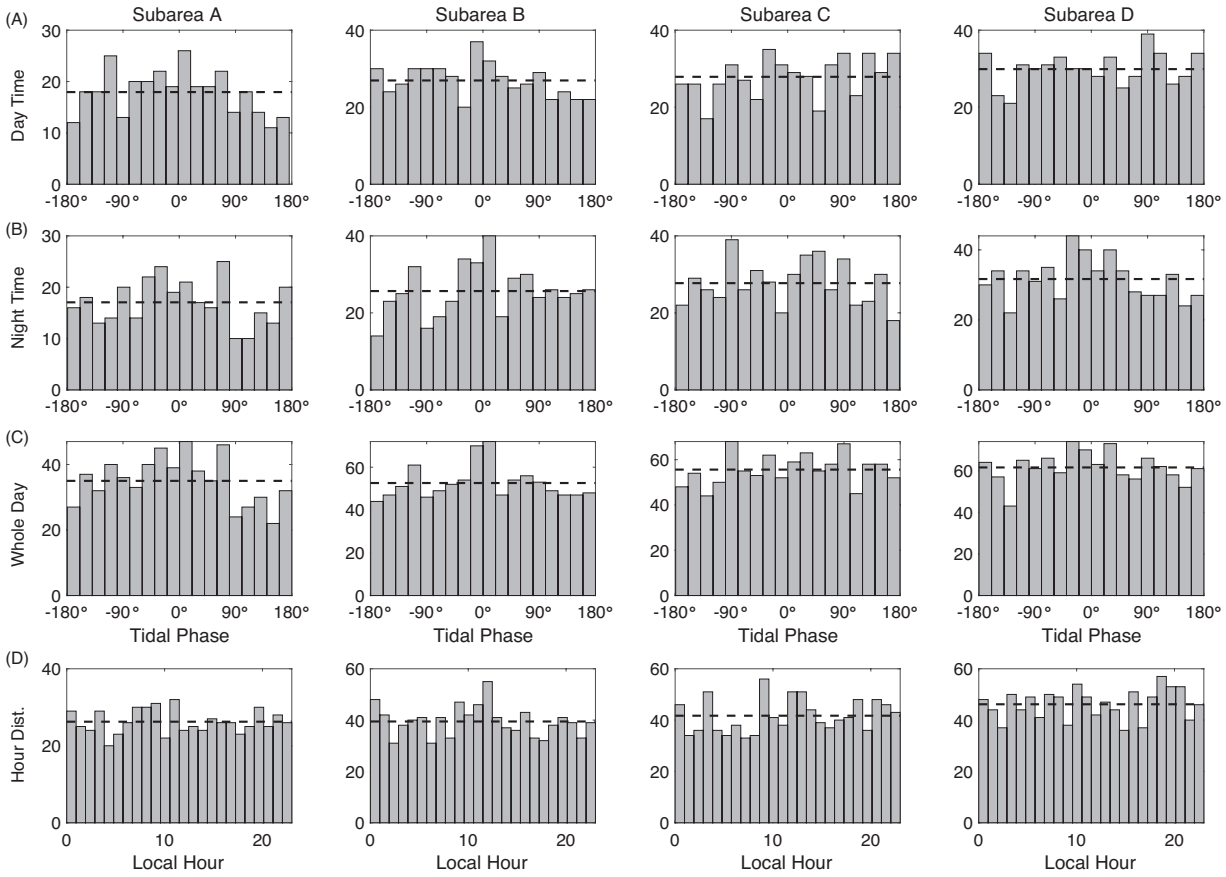

Figure S4. The local day (9:00-21:00) and night (21:00-9:00) distribution of tidal phases for the events in subareas A-D in Figure 3 & 4A. (A)-(C) shows a comparison of the distribution of tidal phases for day, night, and whole day times. (D) shows the distribution of local hour versus event number.

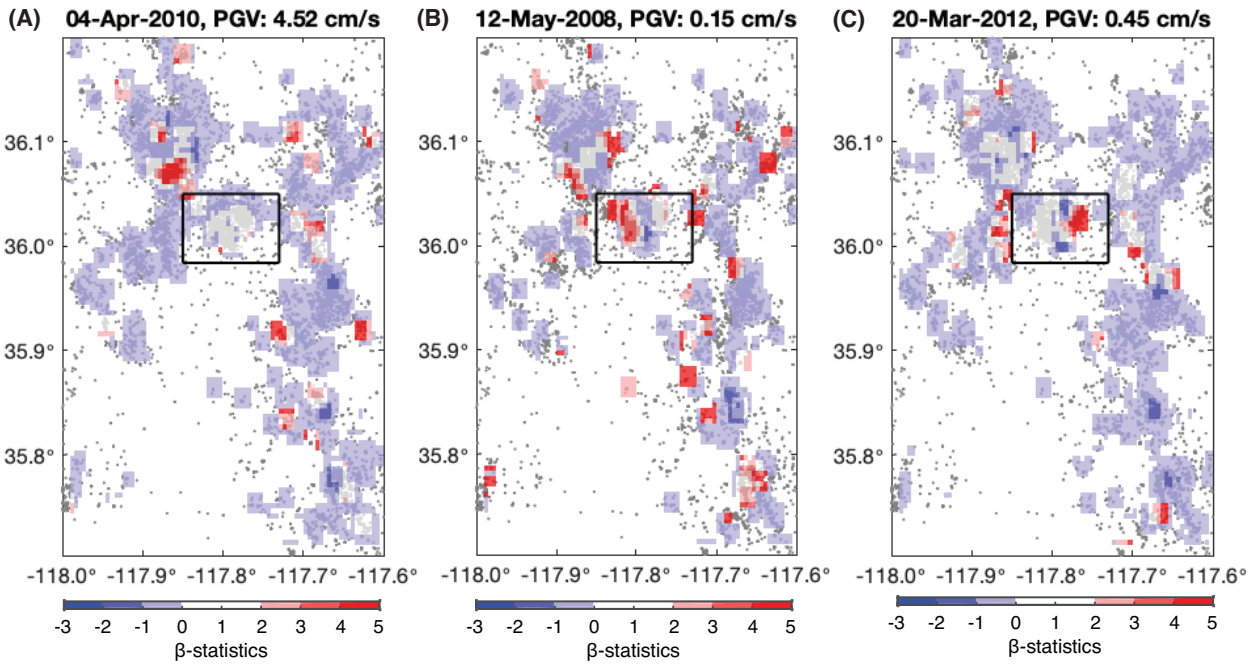

106

107 **Figure S5**. Seismicity rate changes within 10 days following the earthquakes for three representative earthquakes

108 with different remote triggering behavior within the CGF. (A) indicates no seismicity rate change for the 2010 El

109 Mayor-Cucapah earthquake, which generates the largest seismic amplitude within the CGF. (B) and (C) shows

110 the seismicity rate changes for the 2008 Wenchuan and 2012 Oaxaca earthquakes.

111

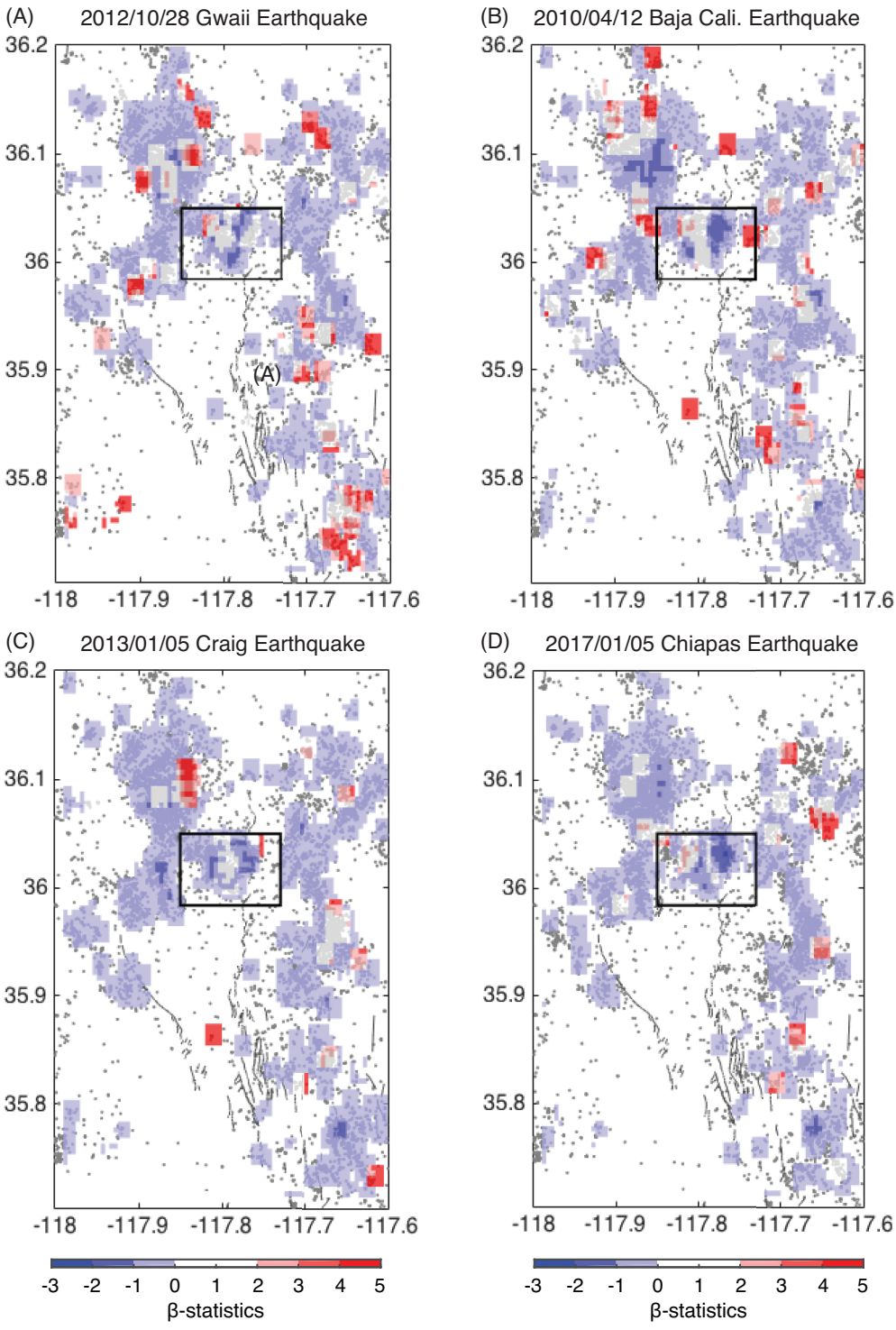

Figure S6. Estimates of seismicity rate changes within 10 days following the earthquakes for the 2010 Gwaii, 2012 Baja California, 2013 Craig, and 2017 Chiapas earthquakes.

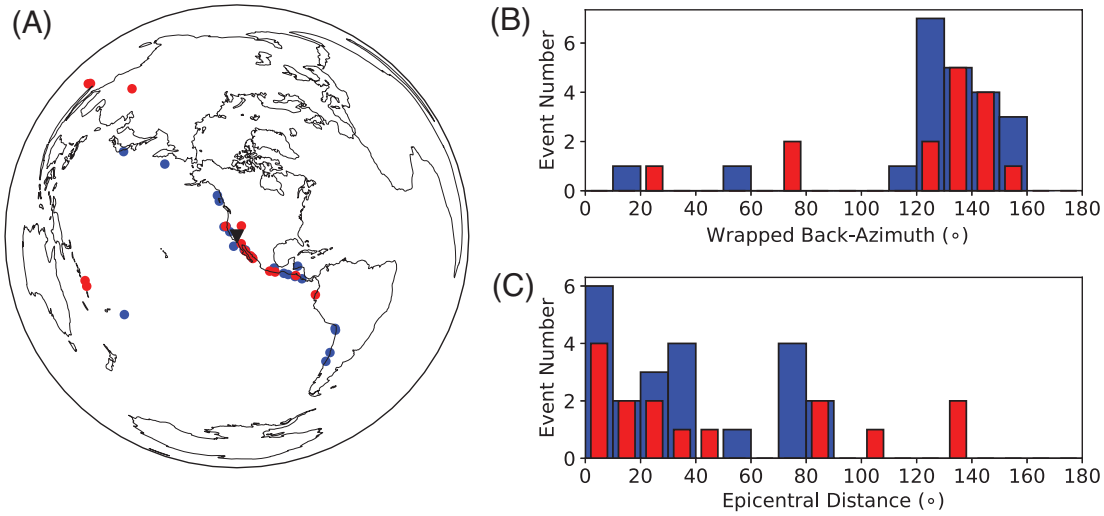

Figure S7. Observations of remote triggering within the CGF. (A) shows the locations of the global events. Red dots show the events with remotely triggered events within the CGF, while the blue dots show those that did not trigger events. The black triangle marks the location of the CGF. (B) & (C) show histograms of the back-azimuths and epicentral distances of the events that remotely triggered events within the CGF (red) compared to those that did not (blue).

Table S1

Table S1. Earthquakes in this study

Date	UTC Time	Ms	Latitude	Longitude	Depth (km)	Location	Peak Amp. (mm/s)
2010/04/04	22:40:43.0	7.3	32.30°	-115.27°	6	El Mayor-Cucapah, Mexico	4.52
2012/04/12	07:15:48.5	7.0	28.70°	-113.10°	13	Baja California, Mexico	0.75
2012/10/28	03:04:08.8	7.8	52.79°	-132.10°	14	Gwaii, Haida	1.14
2013/01/05	08:58:19.3	7.7	55.39°	-134.65°	10	Craig, US	0.72
2017/09/08	04:49:19.2	8.2	15.02°	-93.90°	47	Chiapas, Mexico	1.42
2008/05/12	06:28:01.6	8.1	19.0°	103.32°	19	Wenchuan, China	0.15
2012/03/20	18:02:47.5	7.6	2.33	93.06	20	Oaxaca, Mexico	0.45

Reference

1. Alfaro-Diaz, R., Velasco, A. A., Pankow, K. L., & Kilb, D. (2020). Optimally Oriented Remote Triggering in the Coso Geothermal Region. *J. Geophys. Res.: Solid Earth*, *125*(8), 1–18.
2. Kaven, J. O. (2020). Seismicity Rate Change at the Coso Geothermal Field Following the July 2019 Ridgecrest Earthquakes. *Bull. Seismol. Soc. Am.*, *110*(4), 1728–1735.
3. Lay, T., and T. C. Wallace (1995), *Modern Global Seismology*, Academic Press, London.

4. Matthews, M. V., and P. A. Reasenberg (1988). Statistical methods for investigating quiescence and other temporal seismicity patterns. *Pure and Appl. Geophys.*, *126*(2–4), 357–372.

5. Reasenberg, P., and W. Simpson (1992). Response of regional seismicity to the static stress change produced by the Loma Prieta earthquake. *Science*, 255(5052), 1687–1690.